1-1-2020

Myosin V-mediated transport of Snc1 and Vps10 toward the trans-Golgi network

Vy Nguyen
MSU Graduate Student

Jared Smothers
MSU Undergraduate

Paul Ballhorn
MSU Graduate Student

Sravya Kottapalli
MSU Graduate Student

Anh Ly
MSU Graduate Student

See next page for additional authors

Recommended Citation

Nguyen, Vy, Jared Smothers, Paul Ballhorn, Sravya Kottapalli, Anh Ly, Julia Villarreal, and Kyoungtae Kim. "Myosin V-mediated transport of Snc1 and Vps10 toward the trans-Golgi network." European Journal of Cell Biology (2020): 151143.

European Journal of Cell Biology xxx (xxxx) xxx

Contents lists available at ScienceDirect

European Journal of Cell Biology

journal homepage: www.elsevier.com/locate/ejcb

Research paper

Myosin V-mediated transport of Snc1 and Vps10 toward the *trans*-Golgi network

Vy Nguyen [a], Jared Smothers [a,b], Paul Ballhorn [a], Sravya Kottapalli [a], Anh Ly [a], Julia Villarreal [a], Kyoungtae Kim [a,*]

[a] Department of Biology, Missouri State University, 901 S National, Springfield, MO, 65807, USA
[b] Department of Biophysics, University of Texas Southwestern Medical Center, 5323 Harry Hines Blvd., Dallas, TX, 75235-8816, USA

ARTICLE INFO

Keywords:
ATPase
Intracellular trafficking
Myosin
Snc1
Time-lapse images
Vps10

ABSTRACT

Retrieval of cargo proteins from the endosome towards the *trans*-Golgi network (TGN) is a crucial intracellular process for cellular homeostasis. Its dysfunction is associated with pathogenesis of Alzheimer and Parkinson's diseases. Myosin family proteins are cellular motors walking along actin filaments by utilizing the chemical energy from ATP hydrolysis, known to involve in pleiotropic cellular trafficking pathways. However, the question of whether myosins play a role in the trafficking of Snc1 and Vps10 has not been addressed yet. The present study assesses the potential roles of all five yeast myosins in the recycling of two membrane cargo, Snc1 and Vps10. It appears that all myosins except Myo2 are not required for the Snc1 traffic, while it was found that Myo1 and 2 play important roles for Vps10 retrieval from the endosome and the vacuole. Multiple *myo2* mutants harboring a point mutation in the actin binding or the cargo binding tail domain were characterized to demonstrate abnormal Vps10-GFP and GFP-Snc1 distribution phenotypes, suggesting a severe defect in their sorting and trafficking at the endosome. Furthermore, Vps10-GFP patches in all tested *myo2* mutants were found to be near stationary with quantitative live cell imaging. Finally, we found that actin cables in the *myo2* mutant cells were considerably disrupted, which may aggravate the trafficking of Vps10 from the endosome. Together, our results provide novel insights into the function of Myo-family proteins in the recycling traffic of Vps10 and Snc1 destined for the TGN.

1. Introduction

Myosins are a large family of motor proteins that interact with actin and use the energy driven by ATP hydrolysis to function for a spectrum of biological processes including intracellular trafficking, muscle contraction, and cell motility (Ryan and Nebenfuhr, 2018). Regardless of their types, the head domain of all myosins bind to filamentous actin and ATP, and the coiled-coil tail domain is able to interact with a variety of cargo molecules (Buss and Kendrick-Jones, 2011). *Saccharomyces cerevisiae*, the budding yeast, expresses 5 myosins, Myo1, Myo2, Myo3, Myo4, and Myo5 (Brown, 1997). Myo1 is a type II myosin that plays a pivotal role in cytokinesis (Lister et al., 2006; Lord et al., 2005), for which it appears that the C-terminal tail region of Myo1 exerts more important roles than the N-terminal motor domain (Lister et al., 2006; Santiago et al., 2016). Budding yeast Myo2 and Myo4 are class-V myosins, which serve as motors that function as vehicles that transport intracellular cargoes via actin filament-dependent motility (Pollard and Lord, 2014). Similar to mammalian myosin V, Myo2 in *S. cerevisiae* is responsible for delivering a wide spectrum of organelles and secretory membranes to the daughter cell (Bretscher, 2003). The other type V myosin in the budding yeast is Myo4, a well-known motor protein that transports *ASH1* mRNA to the growing bud (Jansen et al., 1996). Further investigations showed that at least two more proteins, including She2 and She3, work together to facilitate the transport of *ASH1* mRNA (Bohl et al., 2000; Long et al., 2000). Finally, the budding yeast contains two class I myosins, Myo3 and Myo5, both of which are implicated in facilitating earlier steps of the receptor mediated endocytic pathway (Galletta et al., 2008; Lewellyn et al., 2015) by serving as an actin nucleation-promoting factor (NPF) (Kaksonen et al., 2005).

Many intracellular trafficking pathways depend on actin filament-based myosin motility. However, specific types of myosin motors implicated in the retrograde traffic from the endosome to the *trans*-Golgi network (TGN) have not been characterized yet. One of the most effective strategies to assess the significance of a protein factor

* Corresponding author.
E-mail address: kkim@missouristate.edu (K. Kim).

https://doi.org/10.1016/j.ejcb.2020.151143
Received 25 November 2019; Received in revised form 30 October 2020; Accepted 27 November 2020
Available online 30 November 2020

implicated in the retrograde traffic would involve a quantitative measurement of defects in delivery of cargoes destined for the TGN in cells lacking the protein factor or in cells expressing a mutated version of the factor. Two well-known cargoes for the traffic pathway are Snc1 and Vps10. The former is a v-SNARE, which is synthesized in endoplasmic reticulum (ER) and is targeted to the plasma membrane. Recycling of Snc1 is a complex process that involves endocytosis, retrograde trafficking from the early endosome to the TGN, and secretion back to the plasma membrane, primarily in the daughter membrane when the retrograde or recycling traffic is functional (TerBush et al., 1996; Woodman and Kim, 2018). The carboxypeptidase Y (CPY) receptor Vps10 shuttles between the late endosome and the TGN (Marcusson et al., 1994), thereby serving as a reporter for the retrograde traffic toward the TGN. The present study sought to identify specific types of myosin implicated in the retrograde traffic by examining proper recycling of GFP-Snc1 and Vps10-GFP toward the TGN. Our results here show that Myo2 is the key player on this traffic and that both the N-terminal actin binding domain and the C-terminal tail domain are required for optimal traffic of Snc1 and Vps10. Further, we show that Vps10 exhibits reduced range of motion by a substitution of specific residues of Myo2. Additionally, actin cables are disrupted as small fragments, and actin patches are depolarized in *myo2* mutant cells.

2. Materials and methods

2.1. Yeast strains and plasmids

All yeast mutant strains and plasmids used for this study are listed in Tables 1 and 2, respectively. *MATα ura3 his2 leu2−3,112 trp1−1 ade1 MYO1*Δ::*URA3* (KKY1909) strain was a gift from Dr. Rong Li (John Hopkins School of Medicine) (Tolliday et al., 2003). *MATα his3*Δ*1 leu2*Δ*0 met15*Δ*0 ura3*Δ*0* (KKY 0002), *MATα leu2*Δ*0 met15*Δ*0 ura3*Δ*0 MYO3*Δ::*KanMX* (KKY 1963) and *MATα leu2*Δ*0 met15*Δ*0 ura3*Δ*0 MYO5*Δ::*KanMX* (KKY 1964) strains were purchased from Invitrogen. *MATα his3*Δ*1 leu2*Δ*0 ura3*Δ*0 met15*Δ*0 MYO4*Δ::*KanMX* (KKY 1935) strain was gotten from Euroscarf. *MATα his3 leu2 trp1 bar1 myo3*Δ::*HIS3 myo5*Δ::*TRP1* [*myo5−1 URA3*] (KKY 1924) strain was given as a gift by Dr. Spudich from Stanford University (Goodson et al., 1996). *MATα ade2−101 his3*Δ*200 leu2−3,112 lys2−801 ura3−52 myo2−16*::*HIS3* (KKY 1923) and *MATα ade2−101 his3*Δ*200 leu2−3,112 lys2−801 ura3−52 myo2−66*::*HIS3* (KKY 1922) strains were donated by Dr. Bretscher from Cornell University (Schott et al., 1999). PTPI1-GFP-SNC1 (pm) URA3 CEN (KKD 0062) and P_{TPI1}-GFP-SNC1 LEU2 CEN (KKD 0064) plasmids were contributed by Dr. Tanaka from Hokkaido University (Furuta et al., 2007). pAD54-HA VPS10-GFP (KKD 0333) plasmid was received as a gift from Dr. Gerst from Weizmann Institute of Science (Kama et al., 2007). pRS413-*myo2*-1114−1519 HIS3 CEN (KKD 0369), pRS413-*myo2*-1−1345 HIS3 CEN (KKD 0368), pRS413-*myo2−2*-G1248D HIS3 CEN (KKD 0365), pRS413-*myo2*-D1297 N HIS3 CEN (KKD 0363), pRS413-*myo2*-N1304D HIS3 CEN (KKD 0371), pRS413-*myo2*-Y1415R HIS3 CEN (KKD 0364), and pRS413-*myo2*-K1444A HIS3 CEN (KKD 0372) plasmids were the favor from Dr. Lois Weisman (Michigan University Life Science Institute) (Catlett and Weisman, 1998; Eves et al., 2012; Ishikawa et al., 2003; Pashkova et al., 2005b, 2006). Before using them, we sequenced (Eurofins Genomics) and identified the mutated site from the vectors as well as confirmed no additional mutations in each vector (Table 3).

2.2. Cell growth and reagents

Wild-type yeast cells (KKY 0002) were grown in YPD liquid medium (1% bacto yeast extracts, 2% bacto peptone, and 2% glucose). A variety of *myo2* mutant strains were grown in appropriate media, including -URA (lacking Uracil), -LEU (lacking Leucine), -HIS (lacking Histidine), 5-FOA-His (5-fluoroorotic acid and lacking Histidine), -HIS-LEU (lacking both Histidine and Leucine), and -HIS-URA (lacking both Histidine and

Table 1
Yeast strains used in this study.

Strain	Source	Genotype
KKY 0002	Invitrogen	*MATα his3Δ1 leu2Δ0 met15Δ0 ura3Δ0*
KKY 1909	(Tolliday et al., 2003)	*MATα ura3 his2 leu2−3,112 trp1−1 ade1 MYO1*Δ::*URA3*
KKY 1963	Invitrogen	*MATα leu2Δ0 met15Δ0 ura3Δ0 MYO3*Δ::*KanMX*
KKY 1935	Euroscarf	*MATα his3Δ1 leu2Δ0 ura3Δ0 met15Δ0 MYO4*Δ::*KanMX*
KKY 1964	Invitrogen	*MATα leu2Δ0 met15Δ0 ura3Δ0 MYO5*Δ::*KanMX*
KKY 1924	(Goodson et al., 1996)	*MATα his3 leu2 trp1 bar1 myo3*Δ::*HIS3 myo5*Δ::*TRP1 [myo5−1 URA3]*
KKY 1943	(Catlett and Weisman, 1998)	*MATα, ura3−52, leu2−3, his3-Δ200, trp1-Δ901, lys2−801, suc2-Δ9,myo2Δ::TRP1, pRS416-MYO2*
KKY 1942	(Catlett and Weisman, 1998)	*MATα, ura3−52, leu2−3, his3-Δ200, trp1-Δ901, lys2−801, suc2-Δ9,myo2Δ::TRP1, pRS413-MYO2*
KKY 1926	(Catlett and Weisman, 1998)	*MATα ade2−101 his3Δ200 leu2−3,112 lys2−801 ura3−52 MYO2::HIS3*
KKY 1923	(Schott et al., 1999)	*MATα ade2−101 his3Δ200 leu2−3,112 lys2−801 ura3−52 myo2−16::HIS3*
KKY 1922	(Schott et al., 1999)	*MATα ade2−101 his3Δ200 leu2−3,112 lys2−801 ura3−52 myo2−66::HIS3*
KKY 1973	This study	*MATα, ura3−52, leu2−3, his3-Δ200, trp1-Δ901, lys2−801, suc2-Δ9,myo2Δ::TRP1 pRS413-myo2−1114-1519*
KKY 1974	This study	*MATα, ura3−52, leu2−3, his3-Δ200, trp1-Δ901, lys2−801, suc2-Δ9,myo2Δ::TRP1 pRS413-myo2-1−1345*
KKY 1975	This study	*MATα, ura3−52, leu2−3, his3-Δ200, trp1-Δ901, lys2−801, suc2-Δ9,myo2Δ::TRP1 pRS413-myo2−2-G1248D*
KKY 1969	This study	*MATα, ura3−52, leu2−3, his3-Δ200, trp1-Δ901, lys2−801, suc2-Δ9,myo2Δ::TRP1 pRS413-myo2-D1279N*
KKY 1972	This study	*MATα, ura3−52, leu2−3, his3-Δ200, trp1-Δ901, lys2−801, suc2-Δ9,myo2Δ::TRP1 pRS413-myo2-N1304D*
KKY 1970	This study	*MATα, ura3−52, leu2−3, his3-Δ200, trp1-Δ901, lys2−801, suc2-Δ9,myo2Δ::TRP1 pRS413-myo2-Y1415R*
KKY 1971	This study	*MATα, ura3−52, leu2−3, his3-Δ200, trp1-Δ901, lys2−801, suc2-Δ9,myo2Δ::TRP1 pRS413-myo2-K1444A*
KKY 1525	This study	KKY 0002, GFP-Snc1
KKY 1928	This study	KKY 1909, GFP-Snc1
KKY 1978	This study	KKY 1963, GFP-Snc1
KKY 1939	This study	KKY 1935, GFP-Snc1
KKY 1946	This study	KKY 1964, GFP-Snc1
KKY 1937	This study	KKY 1924, GFP-Snc1
KKY 1932	This study	KKY 1923, GFP-Snc1
KKY 1934	This study	KKY 1922, GFP-Snc1
KKY 1951	This study	KKY 1974 x Myo2 (1−1345)-HIS x HA-GFP-Snc1
KKY 1956	This study	KKY 1969 x Myo2 (D1297 N)-HIS x HA-GFP-Snc1
KKY 1957	This study	KKY 1972 x Myo2 (N1304D)-HIS x HA-GFP-Snc1
KKY 1958	This study	KKY 1970 x Myo2 (Y1415R)-HIS x HA- GFP-Snc1
KKY 1981	This study	KKY 1969, GFP-Snc1-pm
KKY 1982	This study	KKY 1971, GFP-Snc1-pm
KKY 1886	This study	KKY 0002, Vps10-GFP
	This study	KKY 1909, Vps10-GFP

(*continued on next page*)

Table 1 (*continued*)

Strain	Source	Genotype
KKY 1927		
KKY 1945	This study	KKY 1963, Vps10-GFP
KKY 1938	This study	KKY 1935, Vps10-GFP
KKY 1980	This study	KKY 1964, Vps10-GFP
KKY 1936	This study	KKY 1924, Vps10-GFP
KKY 1931	This study	KKY 1923, Vps10-GFP
KKY 1933	This study	KKY 1922, Vps10-GFP
KKY 1955	This study	KKY 1973 x Myo2 (1114−1519)-HIS x HA-Vps10-GFP
KKY 1954	This study	KKY 1974 x Myo2 (1−1345)-HIS x HA- Vps10-GFP
KKY 1977	This study	KKY 1975 x Myo2−2 (G1248D)-HIS x HA-Vps10-GFP
KKY 1976	This study	KKY 1969 x Myo2 (D1297 N)-HIS x HA-Vps10-GFP
KKY 1952	This study	KKY 1972 x Myo2 (N1304D)-HIS x HA-Vps10-GFP
KKY 1953	This study	KKY 1970 x Myo2 (Y1415R)-HIS x HA-Vps10-GFP
KKY 1978	This study	KKY 1971 x Myo2 (K1444A)-HIS x HA-Vps10-GFP

Table 2
Plasmid used in this study.

Strain	Source	Description
KKD 0062	(Takeda et al., 2014)	*P_{TPI1}-GFP-SNC1(pm) URA3 CEN*
KKD 0064	(Furuta et al., 2007)	*P_{TPI1}-GFP-SNC1 LEU2 CEN*
KKD 0333	(Kama et al., 2007)	*pAD54-HA VPS10-GFP 2μ LEU2*
KKD 0369	(Pashkova et al., 2005b)	*pRS413-myo2−1114-1519 HIS3 CEN*
KKD 0368	(Pashkova et al., 2005b)	*pRS413-myo2-1−1345 HIS3 CEN*
KKD 0365	(Catlett and Weisman, 1998)	*pRS413-myo2−2-G1248D HIS3 CEN*
KKD 0363	(Ishikawa et al., 2003)	*pRS413-myo2-D1297 N HIS3 CEN*
KKD 0371	(Eves et al., 2012)	*pRS413-myo2-N1304D HIS3 CEN*
KKD 0364	(Pashkova et al., 2006)	*pRS413-myo2-Y1415R HIS3 CEN*
KKD 0372	(Pashkova et al., 2006)	*pRS413-myo2-K1444A HIS3 CEN*

Table 3
DNA sequencing primers used in the study.

Primer	Sequence	Sequencing to check
KKP905	GCGGTGTATTCTGGTTAGCAAACG	Mutations in D1297, C- terminal truncation, and in N1304
KKP906	GTGTTCCATGCTGTAGTCACAACC	Mutations in Y1415 and K1444
KKP907	ACCAGGTGGCAGACTATGAGTCTCC	N-terminal truncation

Uracil).

All plasmids received from the sources above (Table 2) were isolated by following QIAprep® Spin Miniprep Kit protocol (Qiagen). Then, the extracted DNA products were quantitated by using Thermo Scientific™ NanoDrop™ instrument. Approximately 50−100 ng of isolated plasmids was used for one step transformation described below.

2.3. Plasmid shuffling

To replace pRS416-MYO2-URA plasmid with pRS413 plasmids carrying a *myo2* mutant gene in the genetic background of *myo2*Δ, a plasmid shuffle experiment was performed. First, using the one step transformation (Chen et al., 1992), pRS413-*myo2* mutant plasmids (pRS413-*myo2*-1114−1519 HIS3 CEN, pRS413-*myo2*-1−1345 HIS3 CEN, pRS413-*myo2*−*2*-G1248D HIS3 CEN, pRS413-*myo2*-D1297 N HIS3 CEN, pRS413-*myo2*-N1304D HIS3 CEN, pRS413-*myo2*-Y1415R HIS3 CEN, and pRS413-*myo2*-K1444A HIS3 CEN) were introduced to KKY1943 strain harboring pRS416-*MYO2*-URA (Table 1) in -HIS medium, which resulted in partial removal of pRS416-MYO2-URA. To eliminate cells harboring both pRS413-*myo2* mutant plasmids and pRS416-MYO2-URA and keep cells only carrying pRS413-*myo2* mutant plasmids, the positive colonies from the -HIS medium were plated on 5-FOA medium lacking Histidine (5-FOA-HIS). As a result, we created the following 7 strains (KKY 1973, KKY 1974, KKY 1975, KKY 1969, KKY 1972, KKY 1970, and KKY 1971). As shown in Supplementary Fig. 1, some of the positive colonies from –HIS plates grew on –HIS+5-FOA plates. We also plated the positive colonies from the –HIS+5-FOA plate on –URA plates to confirm that all these positive colonies do not contain pRS416-*MYO2*-URA vector (Supplementary Fig. 1). For all these strains, *MYO2* gene was substituted with a TRP auxotrophic maker (See Table 1), and therefore, we also checked if these strains grow on –TRP plate (Supplementary Fig. 1). Among these strains, KKY 1975 is a temperature sensitive mutant (*myo2−2)* expressing *myo2−2^{G1248D}*. The positive colonies from the plate were selected for next round of one step transformation to introduce either (pKT1490 [pRS315 GFP-SNC1] or pAD54-HA VPS10-GFP) (Furuta et al., 2007; Kama et al., 2007). As a result, we created a number of myosin 2 mutant strains expressing either GFP-Snc1 or Vps10-GFP (see Table 1). To measure defects in GFP-Snc1 and Vps10-GFP trafficking, all strains except the temperature sensitive mutant strain were incubated in a shaker at 30 °C prior to fluorescence imaging. For KKY1975 strain, the growth condition was 24 °C initially, and then the temperature was shifted to 37 °C for an hour prior to fluorescence imaging.

2.4. Cell imaging and confocal microscopy

Confocal fluorescent images were taken using a spinning confocal fluorescence microscope equipped with a Yokogawa CSUX1 spinning disk head mounted on an inverted microscope (Olympus IX-81) with a ×100 oil immersion PlanApo objective lens and an ImagEM camera. The exposure time to record GFP-Snc1 and Vps10-GFP fluorescence was set at 100 ms, and camera intensification was 200. The excitation wavelength used for these fluorophores was 488 nm for the GFP channel generated by 3i laser box (Intelligent Imaging Innovations). To visualize GFP-Snc1-pm mutant expressed from P_{TPI1}-GFP-SNC1(pm) plasmid (Table 2), a Leica TCS SPE-II RGBV confocal imaging system with 63X objective lens was used. We chose 488 nm excitation wavelength of the system to excite the GFP for 800 ms.

2.5. Vps10 patch tracking

Time-lapse imaging experiments were conducted by using yeast cells expressing Vps10-GFP with the spinning confocal microscopy system. The exposure time for detecting and recording Vps10-GFP was set to 50 ms. All time-lapse videos were recorded in one minute for total 120 frames (2 frames/second). Only small-budded cells containing Vps10-GFP dots were chosen for further analysis. A regions of interest (ROI) with an applicable cell was cropped and exported to ImageJ (v1.52a) to trace Vps10-GFP motility over time. For this, the “manual tracking” function under “tracking” icon of ImageJ was used to trace x and y coordinates for each individual Vps10-GFP dot over 30 s. These values were transferred to an Excel sheet in order to determine mean squared displacement (MSD) for each Vps10-GFP dot (0.026 μm/pixel). At least 20 Vps10-GFP dots per each strain were chosen to obtain the MSD value for every time point. Finally, all MSD data points were plotted over time (15 s).

2.6. Actin filament staining

Yeast cells including wild type and Myo2 mutant cells were grown in selective media in a 30 °C incubator for 48 h until they reached an OD

between 0.5−0.8. The yeast cells that reached this OD range were then treated with 37 % formaldehyde stock to a final concentration of 4%. The cells incubated with the formaldehyde for ten minutes in order to fix the cells. Then the cells were put into a centrifuge and washed with 1XPBS, and this process was repeated multiple times. Then, the cells were treated with 3.3 μM of Rhodamine-phalloidin and incubated for an hour staining the actin filaments. Then, cells were washed with 1XPBS and ran through a centrifuge in order to get rid of the excess dye. The cells were then visualized with the spinning confocal microscope.

These cells were then put into categories such as polarized, non-polarized, and whether actin filament cables are present or not. Small budded yeast cells were chosen to be analyzed. All polarized cells are denoted by stain cortical actin patches being stained and heavily present in the daughter cell. Non-polarized cells do not have stained actin patches in the daughter cell or contain actin patches that are spread out randomly in the cytoplasm. If filamentous actin cables present in a cell, then they are seen as glowing long red fibers within the cell. The cables visualized were then denoted as fragmented or not. In particular, Myo2 mutant cells displayed fragmented cables that are only present in the mother cell and are sporadically placed. Cables that are not fragmented will connect from the bottom of the daughter cell to the mother cell. Fifty cells were analyzed for the wild type and for each mutant strain during the experiment, and the experiment was repeated three times.

2.7. Statistical analysis

In small budded cells at late G1 stage carrying P_{TPI1}-GFP-SNC1 LEU2 CEN (KKD 0064) plasmid, GFP-Snc1 is localized to the plasma membrane of a growing bud, while cells in other phases of cell cycle do not display this polarized pattern of GFP-Snc1 and are called non-polarized cells. GFP-Snc1 in these non-polarized cells are distributed evenly throughout the plasma membrane or found in the cytoplasm much more abundantly than cells at late G1 stage.

In wild-type yeast cells expressing pAD54-HA VPS10-GFP (KKD 0333) plasmid, Vps10-GFP localizes to cytoplasmic puncta, whereas in cells displaying defects in cargo sorting at the endosome Vps10-GFP is mislocalized to the vacuole rim to form a ring-like structure or Vps10-GFP carrying puncta are abnormally enlarged. Cells exhibiting both defective phenotypes are also classified into the category of “abnormal”.

Thirty small budded cells were used to determine the extent of polarization of GFP-Snc1 and the distribution pattern of Vps10-GFP in a triplicate manner (3 repeats of 30 small budded cells). Microsoft® Office Excel was utilized to determine the mean and standard deviation. Pairwise comparisons between means of different groups were performed using a Student’s *t* test (two tails, two-sample unequal variance). The results were reported as p-values. $0.05 < p \leq 0.1$, $0.01 < p \leq 0.05$ and $p \leq 0.01$ are represented with one (*), two (**) and three (***) asterisks, respectively.

3. Results

3.1. The role of myosin family in the recycling traffic toward the TGN

Myosin family proteins are implicated in membrane trafficking pathways (McIntosh and Ostap, 2016; Musch et al., 1997; Trybus, 2008). However, myosin’s roles in trafficking of a diverse range of cargo transport between organelles remain poorly understood. Although a plethora of gene products have been investigated to study the traffic route of Snc1 and Vps10 in yeast cells, myosin’s potential functions in trafficking of these cargo have not been investigated yet. The ν-SNARE Snc1, a well-documented early endosome marker, is synthesized at the ER, shipped to the Golgi, and to the plasma membrane, in particular, to the region of active growth, namely the growing bud. Subsequently, Snc1 is endocytosed and retrieved to the Golgi prior to a return to the plasma membrane (Gerst et al., 1992; Hettema et al., 2003; Ma et al., 2017; Valdez-Taubas and Pelham, 2003). In particular, Snx4 is involved in sorting Snc1 for proper retrieval to the late Golgi as loss of Snx4 causes Snc1 mistargeting to the vacuole (Hettema et al., 2003; Ma et al., 2017). In addition, Takeda et al. (2014) showed that mutants that block the retrograde transport of Snc1 led to accumulation of Snc1 in an endosome-derived membrane. The assessment of distribution defect(s) of GFP-fused Snc1 (hereafter, GFP-Snc1) in cells lacking a functional gene product helps deduce normal function of the gene in the Snc1 trafficking. To this end, we set out to test which myosins are implicated in Snc1 traffic pathways by utilization of GFP-Snc1 expressing cells, including *myo1*Δ, *myo3*Δ, *myo4*Δ, *myo5*Δ, and *myo3*Δ*myo5*Δ. *MYO2* is essential for cell viability, and therefore, we used two *myo2* temperature sensitive mutant strains, *myo2−16* and *myo2−66,* for the same purpose. *myo2−16* and *myo2−66* harbor a mutation in COOH-terminal tail domain and a mutation in the NH_2-terminal motor domain, respectively. These mutants are known to affect adversely on the targeting of Sec4p, a Rab GTPase component of late secretory vesicles, to the developing buds (Lillie and Brown, 1994; Schott et al., 1999; Walch-Solimena et al., 1997). All single myosin knock-out (KO) strains except $myo2^{ts}$ mutant strains displayed polarized GFP-Snc1 at the growing bud, a similar phenotype to that of WT cells. The extent of GFP-Snc1 polarization for WT cells was 82.6 ± 11.3 %, and for strains of *myo1*Δ, *myo3*Δ, *myo4*Δ, and *myo5*Δ the polarization levels were 94.5 ± 5.0 %, 94.4 ± 9.6 %, 88.9 ± 4.7 %, and 93.3 ± 6.5 %, respectively. In contrast, in all *myo3*Δ*myo5*Δ cells GFP-Snc1 was evenly distributed to the plasma membrane (Fig. 1, A&B), indicating defect in endocytosis. This result is agreement in the previous study that revealed the role of Myo3 and Myo5 in endocytosis (Sun et al., 2006). GFP-Snc1 localization patterns in both $myo2^{ts}$ mutants at 24 °C were similar to that of WT cells, whereas levels of GFP-Snc1 polarization in these mutants were drastically reduced after 1 -h incubation at 37 °C (Fig. 1, C& D). In addition to the depolarized distribution pattern of GFP-Snc1, we observed increased number of cytoplasmic GFP-Snc1 puncta (data not shown), suggesting the possibility that *myo2* plays an important role in the retrograde trafficking of Snc1 toward the Golgi. To study whether GFP-Snc1 puncta found in myosin 2 mutant strains are mistargted to mutivesicular body (MVB) or at the vicinity of the vacuole, we performed an FM4−64 chase experiment. After 20 min chase, GFP-Snc1 puncta were partially colocalized with FM4−64 dots, whereas after 60 min chase none of GFP-Snc1 puncta was coincided with FM4−64 dots, suggesting GFP-Snc1 puncta in *myo2* mutant strains are representing early endosome/Golgi instead of representing MVB or late endosomes (Supplementary Fig. 2A), a similar phenotype observed by Takeda et al. (2014). However, the questions of whether GFP-Snc1 dots in the mutant strain indeed represent endosome-derived vesicles need to be addressed. In addition, we measured the degree of GFP-Snc1 recycling defects with the following 4 *myo2* mutant strains: a truncated Myo2 mutant lacking C-terminal half ($myo2^{1-1345}$), and three Myo2 tail mutant strains carrying a point mutation in each ($myo2^{D1297N}$, $myo2^{N1304D}$, *and* $myo2^{Y1415R}$). As shown in supplementary Fig. 3A&B, we observed severe defects of GFP-Snc1 distribution in these strains, comparable to those seen in *myo2−16* strain at the non-permissive temperature (Fig. 1, C&D). Interestingly, we observed a partial polarization of GFP-Snc1 near the end of the bud in $myo2^{1-1345}$ and $myo2^{D1297N}$ strains, as seen in the figure (Supplementary Fig. 3A). However, we put those cells into the category of depolarized cells due to a strong GFP fluorescence in the mother’s membrane. To exclude the possibility that the observed distribution defects of GFP-Snc1 are due to defects in secretory pathway from the TGN to the plasma membrane, we introduced GFP-Snc1(pm), a Snc1 mutant that is targeted to the plasma membrane but not endocytosed (Takeda et al., 2014). As a result, we found that this GFP-Snc1 mutant was properly secreted to the plasma membrane both in WT and four *myo2* mutant strain ($myo2^{D1297N}$, $myo2^{K1444A}$, $myo2^{N1304D}$ and myo^{2-16}) (Supplementary Fig. 3C), suggesting no secretory defects in these *myo2* mutant strains. Furthermore, it does not appear that the majority of GFP-Snc1 puncta in *myo2* mutants do not coincide with the rim or lumen of the vacuole (Supplementary Fig. 1A). Therefore, both

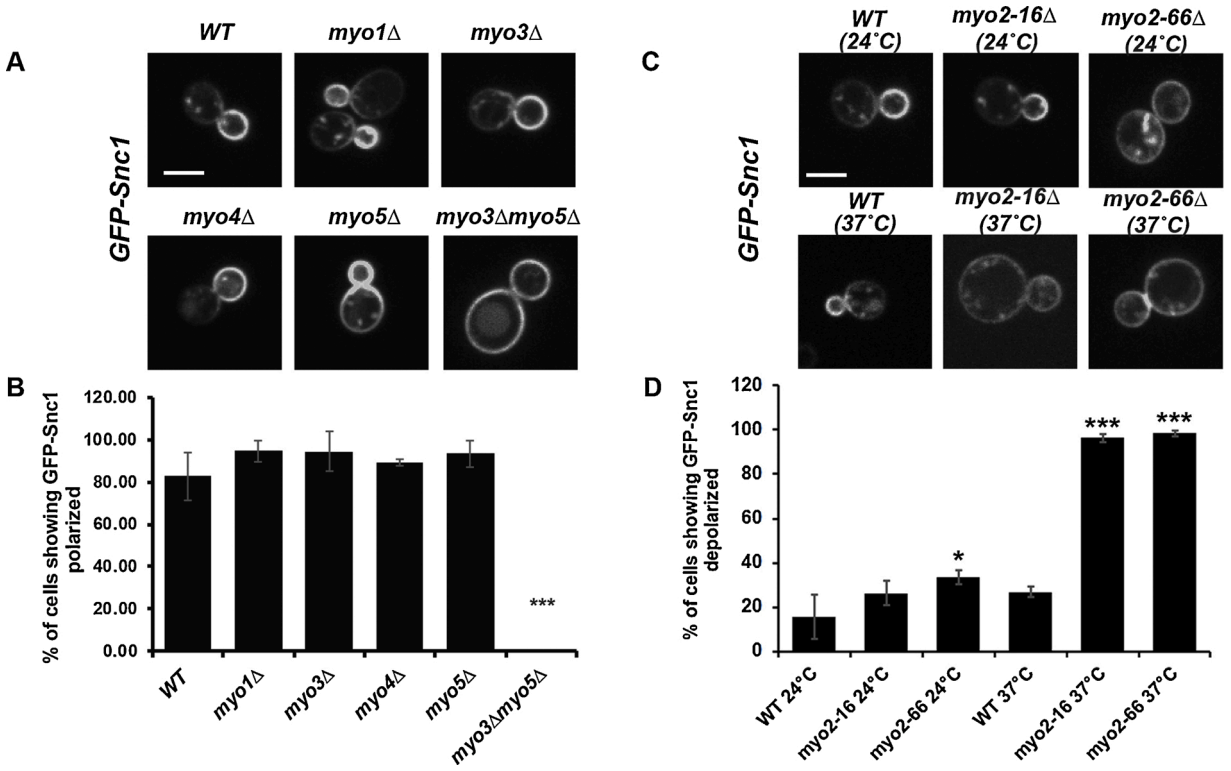

Fig. 1. The effects of myosin knock-out and temperature sensitive mutants on Snc1 polarization. (A) GFP-Snc1 was exogenously expressed in WT, *myo1*Δ, *myo3*Δ, *myo4*Δ, *myo5*Δ and *myo3*Δ*myo5*Δ. Representative pictures of GFP-Snc1 in each strain are shown. (B, D) Percentage of budded cells showing polarized distribution. Levels of GFP-Snc1 polarization in the strains described above were quantified in triplicate manner (3 repeats of 30 small budded cells for each strains). $0.05 < p \leq 0.1$ is indicated with one asterisk and $p \leq 0.01$ is indicated with three asterisks. (C) Representative pictures of GFP-Snc1 pattern shown in WT, *myo2-16*, and *myo2-66* are shown at permissive and restrictive temperature, 24°C and 37°C, respectively. WT, wild type. Bars, 3 μm.

accumulation of GFP-Snc1 cytoplasmic dots and uniformly strained Snc1 at the plasma membrane in *myo2* mutant strains might be mainly due to either slow endocytosis or defects in the Golgi-bound traffic pathway.

3.2. The role of myosin family in the traffic from the Late Endosome to TGNs

Vps10 (vacuolar protein sorting 10), a type I membrane protein, functions in the sorting of carboxypeptidase Y (CPY), a soluble vacuolar hydrolase to yeast lysosome-like vacuole (Cooper and Stevens, 1996). It was presented that CPY from the TGN transits the late endosomal/prevacuolar compartment (PVC) prior to reach the vacuole, and this traffic is referred to as the CPY pathway. Immature CPY binds to Vps10 at the late Golgi, and the resulting complexes are delivered to PVC where CPY dissociates from Vps10. Vps10 then recycles back to the Golgi for additional rounds of sorting (Conibear and Stevens, 1998), and therefore, Vps10 serves an intracellular marker for studying retrograde traffic, especially, from the late endosome to the TGN. According to a previous study, Vps10-GFP is detected as punctate patterns corresponded to Golgi and/or endosome compartments in wild type cells (Burda et al., 2002). However, cells lacking genes for Vps10-GFP traffic toward the TGN displayed Vps10-GFP to the rim of the vacuole, forming bright ring-like structures (Arlt et al., 2015). We assessed distribution defects of Vps10-GFP in cells lacking a myosin gene to reveal normal function of each myosin gene in the Vps10 trafficking. Five myosin knock-out strains and two temperature sensitive myosin 2 mutant strains expressing Vps10-GFP were constructed for this purpose. Cells containing multiple cytoplasmic puncta are determined as normal cells. Cells showing accumulative fluorescence dots or ring-like structures are considered as abnormal cells. WT, all single myosin KO, and a double myosin KO cells except *myo1*Δ showed cytoplasmic Vps10-GFP puncta, an indication of normal phenotypes of Vps10-GFP distribution. The mean percentage of WT, *myo3*Δ, *myo4*Δ, *myo5*Δ, and *myo3*Δ*myo5*Δ cells that showed normal Vps10-GFP distribution pattern was 88.1 ± 2.0 %, 66.1 ± 4.5 %, 77.9 ± 10.9 %, 80.8 ± 3.1 % and 71.8 ± 16.1 %, respectively (Fig. 2, B). Unexpectedly, *myo1*Δ cells showed a significant defect phenotype by having all Vps10-GFP found in the lumen of an organelle (Fig. 2, A&B). We hypothesized that Vps10-GFP in *myo1*Δ is mistargeted to the lumen of vacuole and tested it by incubating the mutant cells with FM4−64 for 60 min. We found that Vps10-GFP was mainly located inside the lumen of vacuole as the vacuolar membrane was labeled with FM4−64 as a ring (supplementary Fig. 2A). Because *myo1*Δ cells missort Vps10-GFP into the vacuole lumen, we further tested if cargos bound for vacuole were disrupted in the mutant. To that end, we have expressed and visualized GFP-Cps1. Both in WT and *myo1*Δ cells GFP-Cps1 was properly located in the lumen of vacuole (Supplementary Fig. 2C). This indicates that Cps1 sorting at the endosomal level is normal in the mutant. The vast majority of *myo2−16* cells (84.1 ± 10.5 %) at 24 °C showed normal Vps10-GFP distribution phenotypes, when compared with WT cells (88.1 ± 2.0 %). At the non-permissive temperature, most of the mutant cells demonstrated one or more ring-like structure containing Vps10-GFP (Fig. 2, C). For *myo2−66* cells, Vps10-GFP ring-like structure was obvious even at 24 °C, and the defect was significantly aggravated at 37 °C (Fig. 2, C&D). We extended our experiment to confirm that the Vps10-GFP ring-like structure represents the vacuolar membrane. As shown in Supplementary Fig. 2A&B, Vps10-GFP fluorescence was coincided with that of FM4−64 in a *myo2* mutant strain ($myo2^{D1297N}$) after a 60 min FM4−64 chase experiment, indicating that Vps10-GFP is accumulated at the vacuolar rim in myosin 2 mutant strains. Together, these results indicate that both Myo1 and Myo2 are implicated in Vps10 trafficking, in particular an early stage of the endosome-to-Golgi pathway.

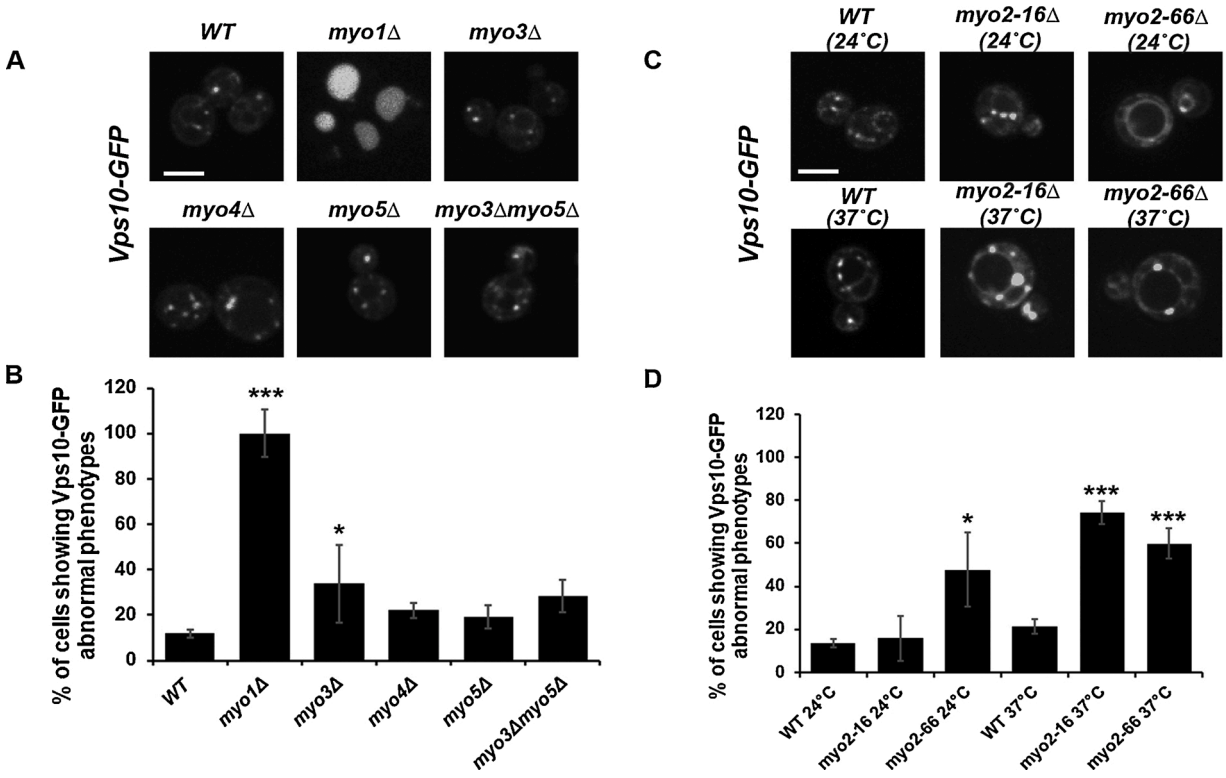

Fig. 2. The effects of myosin knock-out and temperature sensitive mutants on Vps10 distribution pattern. (A) Vps10-GFP was exogenously expressed in WT, *myo1*Δ, *myo3*Δ, *myo4*Δ, *myo5*Δ and *myo3*Δ*myo5*Δ. Representative pictures of Vps10-GFP in each strain are shown. (B) Percentage of budded cells showing abnormal Vps10-GFP distribution. Cells exhibiting enlarged cytoplasmic Vps10-GFP puncta or Vps10-GFP at the vacuolar ring are classified into the group of abnormal phenotype. The strains described above were quantified in triplicate (3 repeats of 30 small budded cells for each strains). $0.05 < p \leq 0.1$ is indicated with one asterisk and $p \leq 0.01$ is indicated with three asterisks. (C) Representative pictures of Vps10-GFP pattern in WT, *myo2-16*, and *myo2-66* are shown at permissive and restrictive temperature, 24°C and 37°C, respectively. (D) Percentage of budded cells showing abnormal Vps10-GFP distribution in WT, *myo2-16*, and *myo2-66* strains. WT, wild type. Bars, 3 μm.

3.3. Cargo-binding domains of myosin 2 functions in traffic of Vps10-GFP

Yeast Myosin 2, a type V myosin motor, is composed of two heavy chains. Each heavy chain is subdivided into four distinct functional domains. The N-terminal motor domain (residues 1 – 1,087) interacts with actin filaments, and this domain is followed by a neck region that has six binding sites (IQ motifs) for calmodulin, the α-helical coiled-coil region that contributes to the dimerization of the heavy chains, and the C-terminal globular tail domain that (residues 1,087 – 1,574) binds cargo (Weisman, 2006). Myosin V motors are able to associate with and transport diverse intracellular cargo, such as secretory vesicles, the vacuole/lysosome, late Golgi elements, peroxisomes, and mitochondria, to distinct destinations in the cell via cargo-specific receptors (Catlett et al., 2000; Catlett and Weisman, 1998; Fagarasanu et al., 2009; Schott et al., 1999; Valiathan and Weisman, 2008). Notably, the distinctive functions of the globular tail in vacuole-specific binding and secretory vesicle-specific binding properties are correlated with two structural subdomains, namely subdomain I (residues 1,087−1,345) and subdomain II (residues 1,346−1,574), respectively (Catlett and Weisman, 1998; Pashkova et al., 2005b; Schott et al., 1999). The functional assessment of various *myo2* point mutations that affect the interaction with the vacuole-specific adaptor protein Vac17 revealed that *myo2*^{D1297N}, *myo2*^{N1304D}, *and myo2*−*2*^{G1248D} (residues on subdomain I) induce defects in vacuole inheritance (Catlett and Weisman, 1998; Eves et al., 2012) (Table 4). In particular, the first two residues, Myo2^{D1297} and Myo2^{N1304}, are on the surface of the subdomain I and implicated in binding to Vac17 directly, while Myo2^{G1248} is buried within the subdomain I, locating apart from the two Vac17 binding residues of Myo2 (Pashkova et al., 2005a, 2006) (Table 4). Similarly, two myosin 2 mutants, *myo2*^{K1444A} *and myo2*^{Y1415R} (residues on subdomain II) cause a failure to translocate secretory vesicles (Donovan and Bretscher, 2012b; Eves et al., 2012; Pashkova et al., 2005a; Santiago-Tirado et al., 2011; Weisman, 2006) (4).

Table 4
Identified defective functions in different mutant myo2 strains.

Mutant residues	Defective function	Sources
2−16 (M1212 T)	Losing the ability in cargo binding, defecting in the distribution of a representative secretory vesicle, Sec4p	(Schott et al., 1999)
2−66 (E511 K)	Losing the ability in movement along actin filament, defecting in the actin patch distribution	(Lillie and Brown, 1994; Schott et al., 1999)
1−1345 (truncation)	Losing function in actin binding and vacuole binding	(Pashkova et al., 2005b)
1114−1519 (truncation)	Losing function in vacuole binding	(Pashkova et al., 2005b)
1248 (G1248D)	Vacuole inheritance dysfunction	(Ishikawa et al., 2003)
1297 (D1297 N)	Vacuole inheritance dysfunction	(Ishikawa et al., 2003)
1304 (N1304D)	Vacuole inheritance dysfunction	(Ishikawa et al., 2003)
1415 (Y1415R)	Vesicle-specific binding dysfunction	(Pashkova et al., 2006)
1444 (K1444A)	Vesicle-specific binding dysfunction	(Pashkova et al., 2006)

The functional assessment of different *myo2* point mutations in the subdomain I, *myo2*^{D1297N}, *myo2*^{N1304D} (point mutations at residues that bind directly to vacuole-specific receptor, Vac17p) and *myo2*−*2*^{G1248D} (locates aside from the region that binds directly to Vac17p) revealed

that these point mutants disrupted vacuole inheritance (Catlett and Weisman, 1998; Eves et al., 2012; Pashkova et al., 2005a, 2006) (Table 4). Similarly, two myosin 2 mutants of subdomain II, *myo2*^{Y1415R} (a point mutant at residue that interact with Rab GTPases Ypt31/32, required for *trans*-Golgi vesicles formation) and *myo2*^{K1444A} (localize to the secretory vesicle-binding region) cause a failure to translocate secretory vesicles (Donovan and Bretscher, 2012b; Eves et al., 2012; Lipatova et al., 2008; Pashkova et al., 2005a; Santiago-Tirado et al., 2011; Weisman, 2006) (Table 4).

To further investigate which domains/residues of Myo2 are required for Vps10-GFP traffic, the same experimental approach shown in the prior section was utilized. All point mutations and truncations in myosin 2 resulted in severe defects in the traffic of Vps10-GFP, manifesting frequent appearance of ring-like structures containing Vps10-GFP. The mean percentage of normal Vps10-GFP distribution in those myosin 2 mutant strains was drastically lower than that of WT cells (Fig. 3, B). Specially, the temperature-sensitive point mutant, *myo2*-2^{G1248D} caused Vps10-GFP localization defects at both permissive and restrictive temperatures. Taken together, these results indicate that myosin 2 tail domain is required for the retrograde trafficking of Vps10.

3.4. Myosin 2 functions in Vps10-GFP motility

We examined the effect of myosin 2 mutants, including two truncated (*myo2*$^{1-1345}$ *and myo2*$^{1114-1519}$) and four point mutants (*myo2*^{D1297N}, *myo2*^{N1304D}, *myo2*$-2^{G1248D,}$ *and myo2*^{Y1415R}), on Vps10-GFP motility by imaging and tracking Vps10-GFP patches. Vps10-GFP patches in WT cells displayed dynamic motility over time. For example, a Vps10-GFP patch in a WT cell moved away quickly from the origin of detection (Fig. 4 and movie 1) and disappeared from the plane of focus. However, the vast majority of Vps10-GFP patches in *myo2*^{Y1415R} cells were stationary at the same location over the full-duration of time-lapse movie (Fig. 4 and movie 2). To define the motile behavior of Vps10-GFP patches in WT and *myo2* mutant cells, we produced MSD (Mean Squared Displacement, μm^2) plots with the function of time. Twenty Vps10-GFP patches per each strain were analyzed, and then the MSD curves at each time point for 15 s are plotted. The averaged Vps10-GFP motility curve from wild type cells indicated an exponential increase in moving distance for approximately 10 s, suggesting a direct motion of these patches, whereas patches in all six myo2 mutant strains appeared to be quite reduced with their corresponding MSD lines nearly parallel to the X-axis (Fig. 5). These results show that functional Myo2 is required for Vps10-GFP motility.

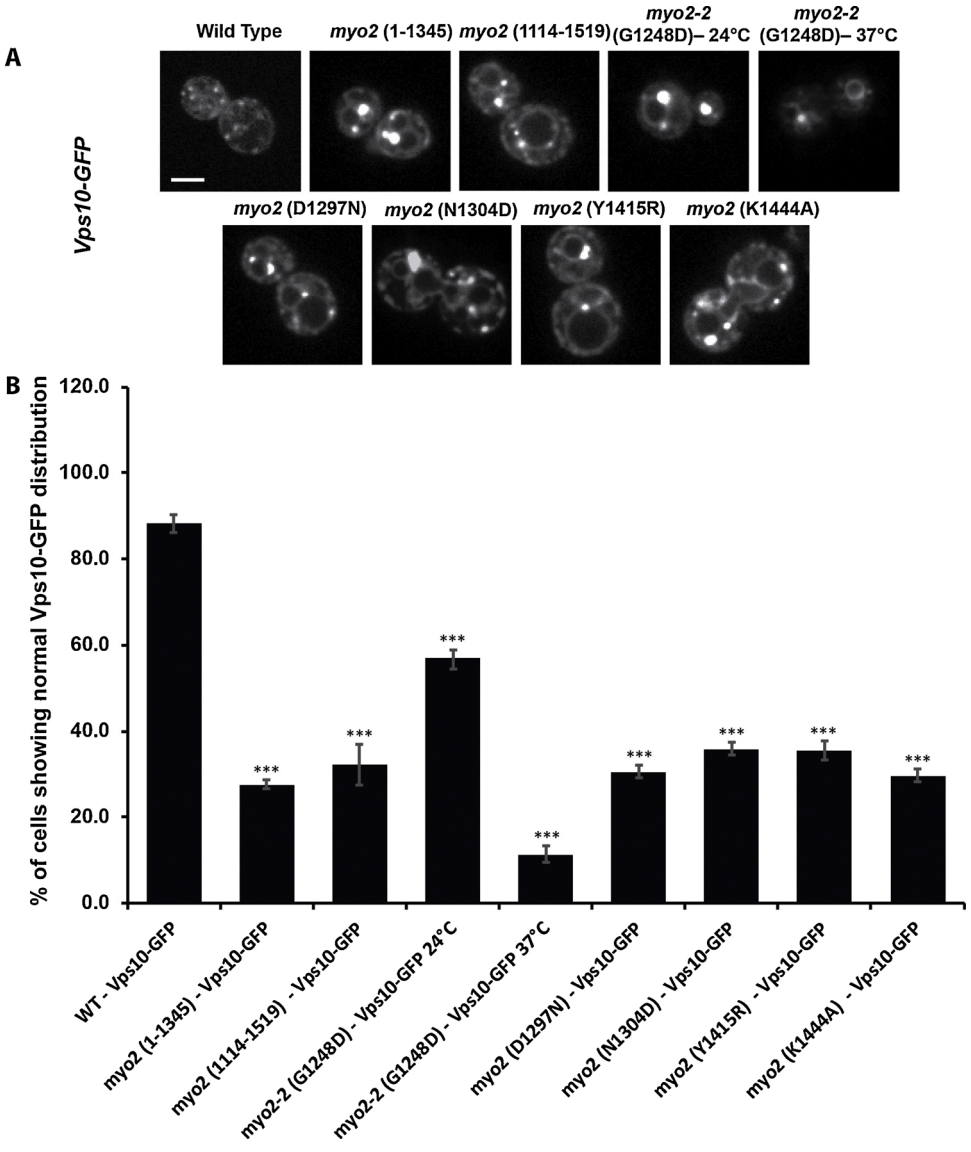

Fig. 3. The effects of mutations and truncations in Myo2 on Vps10 distribution pattern. (A) Vps10-GFP was exogenously expressed in WT, *myo2*$^{1-1345}$, *myo2*$^{1114-1519}$, *myo2-2*^{G1248D}, *myo2*^{D1297N}, *myo2*^{N1304D}, *myo2*^{Y1415R} *and myo2*^{K1444A}. A representative picture of Vps10-GFP for each strain is shown. (B) Percentage of budded cells showing normal Vps10-GFP distribution. As described in Fig. 3 and in the "Methods" section, cells showing Vps10-GFP at the vacuolar ring and enlarged Vps10-GFP puncta are scored into abnormal phenotypes. The strains described above were quantified in triplicate (3 repeats of 30 small budded cells for each strains). $p \leq 0.01$ is indicated with three asterisks. WT, wild type. Bar, 3 μm.

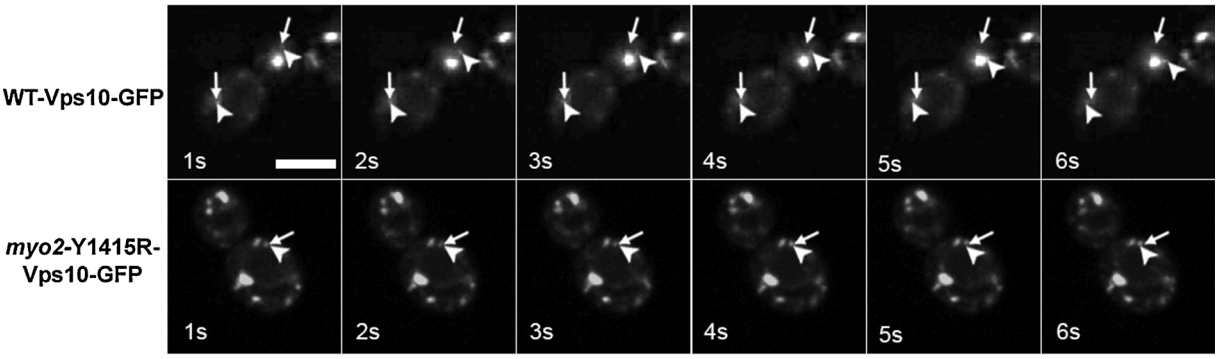

Fig. 4. Time-lapse microscopy of wild-type and *myo2* mutant cells expressing Vps10-GFP. Note the different time intervals between frames in each row. In both wild-type and mutant cells, the arrowhead indicates the starting position of a patch that moves, and the arrow follows the patch. Bar, 3 μm.

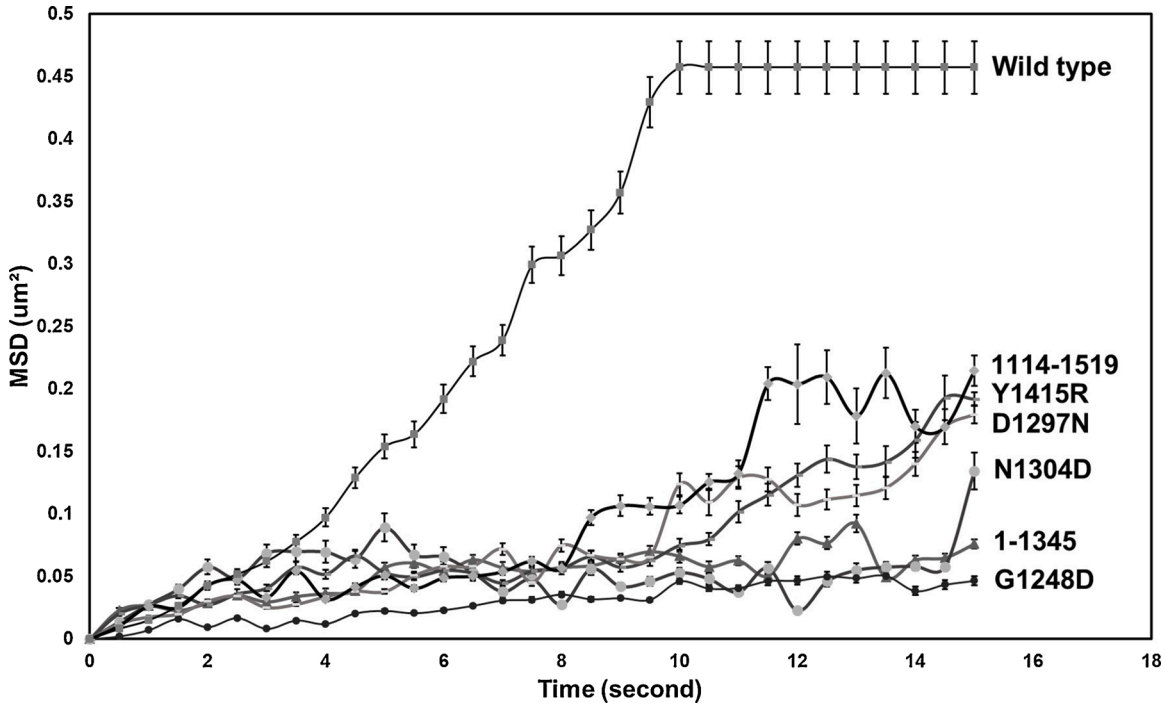

Fig. 5. Mean squared displacement (MSD) of Vps10-GFP patches in wild-type and *myo2* mutant cells. Vps10-GFP patches were tracked up to 15 s before they get invisible. MSD is plotted versus time. The curves are the average of MSD plots of 20 patches from one wild-type and six mutant strains. The experiments were triplicated. Vps10-GFP patches in wild-type cells showed a directed motion represented by a concave up line, whereas the patches were quite stationary in all mutant cells as indicated with lines parallel to the X-axis.

3.5. Myosin 2 mutants display severe disruption of actin cables and cortical actin patches

Actin cables have been known as the cytoskeleton track for polarized trafficking of Myo2. In light of finding a traffic delay of Vps10 in all tested myosin mutant strains, we hypothesized that the actin cable and cortical actin patches are disrupted in our myosin mutant strains. To this end, actin filaments were stained with Rhodamine-phalloidin in order to visualize them under the confocal microscope. Wild type cells expressing functional Myo2 showed intact actin cables that were parallel to the long axis of yeast cell (Fig. 6, A). *myo2* mutant strains such as $myo2^{1-1345}$, $myo2^{1114-1519}$, and $myo2^{Y1415R}$ showed neither actin cables nor fragmented cables. Numerous actin patches were observed instead in those strains. Likewise, the majority of $myo2-2^{G1248D}$, $myo2^{N1304D}$, *and* $myo2^{K1444A}$ strains were observed to have several actin patches without intact or fragmented actin cables. However, these strains rarely contained short, fragmented actin cables (Fig. 6). Further, fragmented actin cables found in these *myo2* mutant cells were observed to be in disarray within the cell. According to our measurement on the extent of actin patch polarization, wild type Myo2 cells were shown to have an average of 65.36 ± 12.1 % of cells that displayed actin patches polarized to the growing bud, whereas the extent of actin patch polarization in all mutant strains was drastically lower: $myo2^{1-1345}$, $myo2^{1114-1519}$, $myo2-2^{G1248D}$, $myo2^{N1304D}$, $myo2^{Y1415R}$ *and* $myo2^{K1444A}$ strains showed 32.7 ± 15.1 %, 28.8 ± 9.6 %, 32.1 ± 9.3 %, 17 ± 21.39 %, 25.8 ± 5.9 %, 16.53 ± 7.9 % of their cells displaying polarization of actin patches (Fig. 6, B). Because all myosin 2 mutant cells displayed varying degrees of actin cable defects, extrapolating the exact role of Myo2 under these conditions would be uneasy. Therefore, we envisioned to explore the potential role of actin cables in the trafficking of Vps10. To that end, we expressed Vps10-GFP in *bnr1Δbni1−12* strain that lacks *BNR1* gene and expresses mutated *BNI1* gene. The actin cable mutant cells exhibited no actin cable not only at the non-permissive temperature (37 °C) but also in a permissive temperature (30 °C) (Supplementary Fig. 4). Under both temperature conditions, the mutant cells displayed an increase in numbers of Vps10-GFP puncta (Supplementary Fig. 4), without showing

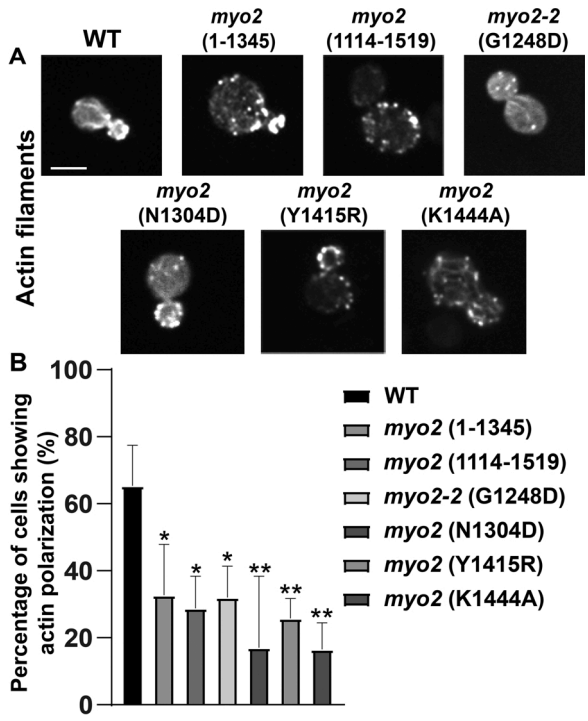

Fig. 6. The effects of Myo2 mutations and truncations on polarization of actin filaments. (A) Imaging the polarized and depolarized actin patches in Wild type and *myo2* mutant cells, respectively. (B) The percentage of cells showing polarized actin patches toward the bud. At least 50 small budded cells in a triplicate manner for each strain were analyzed to obtain the mean and the standard deviation shown in the graph. $0.05 < p \leq 0.1$ is indicated one asterisk, $0.01 < p \leq 0.05$ is indicated two asterisks. WT, wild type. Bar, 3 μm.

bright dots nor ring-like structure containing Vps10-GFP observed in *myo2* mutant cells. Therefore, complete loss of actin cables are not responsible for accumulation of Vps10 at the vacuolar rim or late endosomes. From this finding, we came to the conclusion that Myo2 plays a more important role in retrieving Vps10 from the endosome and the vacuole than actin cables.

4. Discussion

The roles of *S. cerevisiae* Myo2 in vacuole inheritance and secretory pathway have been extensively investigated. However, addressing the question of whether this motor protein contributes to the retrieval of cargo proteins toward the TGN requires more scientific evidence. With that purpose in mind, the present study was set up for the first time examining the implications of all 5 yeast myosin motors in the recycling of Snc1 and Vps10 proteins. Our finding may shed a new light on unknown functions of myosin family in retrograde pathway toward the TGN.

4.1. Myo1 in the traffic of Vps10 toward TGNs

The role of Myo1, a type II myosin family, in the budding yeast has been characterized for cytokinesis and cell division based on several studies in which the disruption of Myo1 resulted in strong cytokinesis defects as well as a delay in cell separation (Lister et al., 2006; Schmidt et al., 2002; Tolliday et al., 2003). Therefore, the mistargeting of Vps10-GFP to the vacuole lumen (Supplementary Fig. 2A) observed in our *myo1*Δ strain may provide hints on yet unidentified functions of Myo1 in Vps10 sorting and trafficking. Along with its well-known route of traffic between the late endosome and TGN, Vps10 also localizes to the vacuolar rim prior to its retrieval toward the TGN (Arlt et al., 2015; Suzuki and Emr, 2018). However, the GFP fluorescence in the *myo1*Δ cells are found to be in the lumen of the vacuole, indicating a severe sorting defect at the late endosome or/and the vacuolar rim. It is not clear whether this sorting defect is due to an indirect or direct effect of dysfunctional cytokinesis in the absence of Myo1. It is well known that Myo1 is targeted to the site of cytokinesis and dissociates from it upon completion of cytokinesis (Richman et al., 2002). Nevertheless, we can not exclude the possibility that a minor fraction of cytoplasmic Myo1 whose concentration might be under the detection limit via a microscopic method can be recruited to the endosome for the yet unidentified function of sorting Vps10. Given that the abnormal localization Vps10-GFP inside the vacuole is observed throughout the cell cycle (data not shown) in cells lacking Myo1, the above-mentioned possibility of Myo1 association with the endosome is likely. Nevertheless, we speculate that the abnormal targeting of Vps10-GFP in the *myo1* mutant cell has nothing to do with the function of ESCRT the sorting machinery responsible for loading receptor proteins into the intraluminal vesicle. It is because GFP-Cps1 targeting to the vacuole lumen in *myo1*Δ cells was not compromised when compared to that of WT cells (Supplementary Fig. 2C). Further, the prolonged existence of Vps10-GFP fluorescence in the vacuolar lumen (Fig. 2A and Supplementary Fig. 2A) suggests an alteration of the internal environment into a less acidic condition in which hydrolysis-based protein degradation activities are not optimal. Alternatively, it is possible that the Vps10 portion from the fusion protein would be vulnerable to the hydrolytic activity in the lumen, but the GFP portion might be stable in the condition, which could explain the prolonged fluorescence in the lumen. Interestingly, the GFP-Snc1 distribution pattern in *myo1*Δ cells were comparable to that of wild type cells, suggesting that Snc1 sorting and trafficking is independent of Myo1 function. Taken together, it is likely that Snc1 and Vps10 at the endosome are differently handled by their specific sorting machinery, and the potential function of Myo1 for assisting Vps10 sorting and trafficking is of great interest for an investigation.

4.2. Myo2 functions in Vps10 retrograde pathway

Retrieval of Vps10 to the Golgi is known to depend on the retromer complex, a group of proteins regulating the recycling of various cargo from the endosome to TGN (Vagnozzi and Pratico, 2019). Normally, Vps10-GFP is found as puncta in the cytoplasm, marking endosomes and the late Golgi, as shown previously (Chi et al., 2014; Piper et al., 1995). The dysfunction of retromer complex leads to a significant defect in Vps10 retrieval from endosomes and the vacuole, manifested by the presence of large cytoplasmic Vps10-GFP puncta and ring-like structures carrying Vps10-GFP (Arlt et al., 2015; Burda et al., 2002). Based on our observations of the abnormal Vps10-GFP distribution pattern resembling that of retromer mutant cells, we put forth a model that depicts the potential consequence of the presence of functional Myo2 or a mutated *myo2* variant (Fig. 7). To our knowledge, the interaction between Myo2 and Vps10 has not been documented yet, but the myosin tail is known to bind to a diverse range of membranes by the aid of a membrane-specific adaptor or through the direct interaction between Myo2 tail and the cargo membrane (Jin et al., 2011; Winding and Gelfand, 2014; Yau et al., 2014). Furthermore, it was proposed that the actin filaments surrounding the Golgi complex have their plus ends toward the membrane and their minus ends pointing away (Warner et al., 2003). Therefore, we propose that Myo2 is able to interact with endosome or vacuole-derived vesicles, regardless of their interaction modes, and walks along the actin cable toward the Golgi, near which the positive end of actin cable may concentrate for efficient docking of transported membrane cargo to a cargo entry site (Fig. 7, A). In wild type cells, a minor fraction of Vps10 receptors are sorted into intraluminal vesicles (ILVs) that are destined for degradation in the vacuole, whereas the vast majority of them are retrieved to the Golgi from the late endosome and the vacuole (Nickerson et al., 2010) (Fig. 7). In light of finding that *myo2* mutant cells exhibiting several large Vps10-GFP fluorescent dots and ring-like structures with Vps10-GFP (Figs. 2, C and 3, A), we came to the

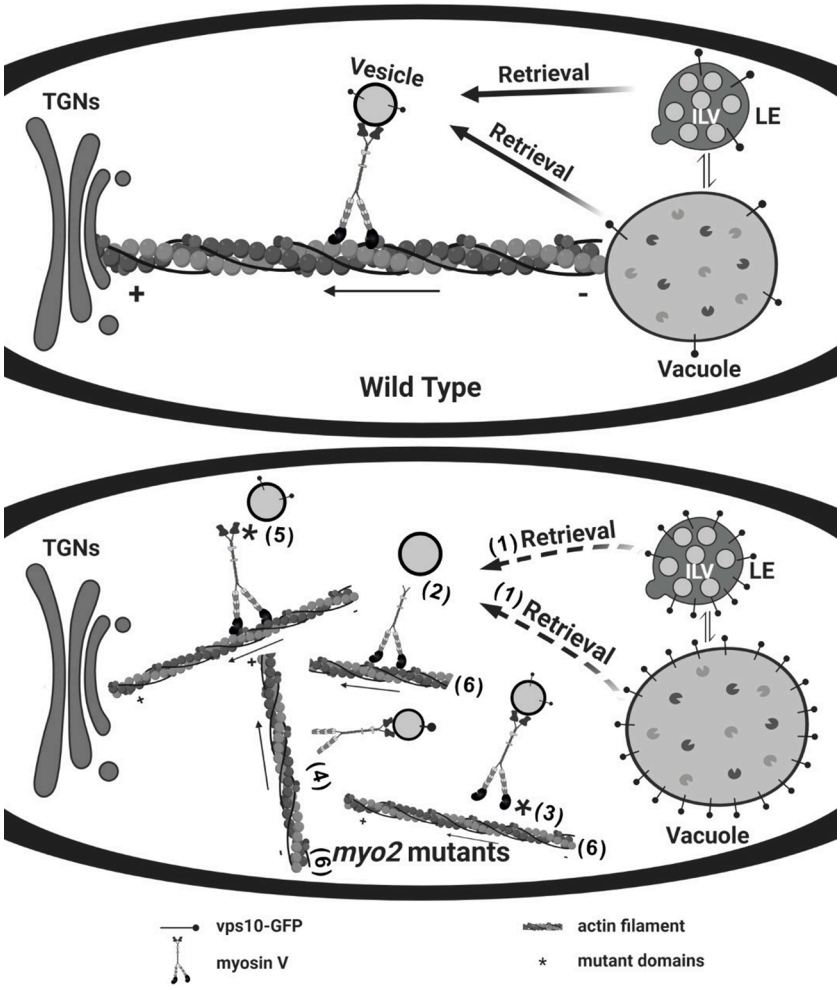

Fig. 7. Diagram summarizing the potential consequence of Vps10 in the presence of functional Myo2 (top) and mutant *myo2* (bottom). (Top) Myosin 2 moves along actin filament and delivers endosomal vesicle to TGNs. (Bottom) (1) Endosomal vesicles are inefficiently retrieved. (2) *Myo2* tail domain mutation is unable to bind to the vesicle. (3) *Myo2* mutants harboring a point mutation in its head bind the actin filament in an inefficient manner. (4) *myo2* mutant lacking its N-terminal actin biding domain truncation is unable to associate with actin filament. (5) *Myo2* head domain point mutation, resulting in a weak interaction with the cargo vesicle. (6) Disrupted actin cable that cripples the migration of *myo2* mutant motors.

conclusion that earlier stages of Vps10 retrieval, such as its sorting and loading to correct membrane vehicles or vesicles, at the endosome and the vacuole are significantly disrupted (Fig. 7, B). On the basis of our observation of enlarged Vps10-GFP puncta in *myo2* mutant cells (Figs. 2 and 3), we also proposed the possibility that the endosomal sorting complex retromer might not function properly in the absence of intact Myo2. This idea is consistent with the previous investigation that reported defective retromer functions in cells manifesting enlarged Vps10-GFP puncta in mutant fission yeast cells (Yanguas et al., 2019). It appears that there is a positive correlation between this abnormal Vps10-GFP accumulation and the severity of actin cytoskeleton organization (Figs. 2,3, and 6), which provides hints of certain unknown functions of the acto-myosin system for organizing the proper structure of its interacting endosome. Yet, the questions of whether the enlarged Vps10-GFP puncta present late endosome itself is of interest to be explored. Furthermore, it is highly likely that *myo2* truncated mutants, lacking either a portion of its tail or motor domain (Figs. 3 and 6), would not bind their cargo membrane or the actin cable in an effective manner, respectively, resulting in a severe cargo traffic delay (Fig. 7, B). Similar defective phenotypes of Vps10-GFP shown in the truncated *myo2* mutant cells were also found in *myo2* point mutants whose functions are related to vacuole inheritance or secretory vesicle traffic pathways. These results are the first evidence that highlights the key function of Myo2 in delivering Vps10 to TGN.

4.3. *Vps10-GFP motility affected by myo2 mutations*

Time-lapse fluorescence imaging techniques in conjunction with moving-patch analysis have provided significant insights into understanding the nature of motile vesicles, including endocytic and exocytic vesicles, defining if they undergo either a directed or a random motion inside the cell. Nevertheless, the characteristic motile behavior of Vps10-carrying vesicles has been overlooked. As such, to our knowledge, we are the first group revealing that Vps10-GFP patches under normal conditions manifest a type of directed motion until they disappear from the focused field of view. Myo2 is proposed to function in directed transport of its cargo along the actin filament toward its positive end with the average moving velocity of 0.2−0.5 μm/s, by the use of fluorescence live imaging methods (Pierobon et al., 2009). Myo2 is also thought to be associated with secretory vesicles of GFP-Sec4 through direct interaction between Myo2 and Sec4, and the measured velocity of the cargo was approximately 3 μm/s (Donovan and Bretscher, 2012a; Jin et al., 2011; Schott et al., 2002). The discrepancy in moving speeds by myo2-mediated motility has been attributed to the lack of full capability of direct single-molecule measurements (Kodera and Ando, 2014; Pierobon et al., 2009). The mean velocity of Vps10-GFP patches in our experiments was approximately 0.21 μm/s while they exhibited a directed motion, which is comparable to the range of above-mentioned Myo2 velocity. Just because Vps10-GFP moves in a similar speed of Myo2, that does not necessarily serve as the direct evidence that the cargo is delivered via Myo2 motor. Further investigations using higher spatial and temporal resolution microscopy will help characterize whether Myo2 indeed carries Vps10 to the final destination. On the contrary, the majority of Vps10 patches in mutant cells exhibited a stationary behavior, consistent with abnormal accumulation of Vps10-GFP as cytoplasmic puncta. It is possible that Vps10 molecules

are trapped in the endosomes as well as at the vacuolar rim, or that Vps10-bearing vesicles ineffectively interacts with mutant *myo2*. However, it is not conclusive if the enlarged Vps10-GFP puncta are vesicles derived from the endosome or endosome itself.

Declaration of Competing Interest

The authors report no declarations of interest.

Acknowledgement

This work was supported by a Faculty Research Grant (to K. Kim) and by thesis funding from Missouri State University (to V.Nguyen). V. Nguyen contributed to the preparation of the figures and substantially contributed to the writing of this manuscript. K. Kim provided the intellectual input and participated in the manuscript correction, proofreading, and revision of the manuscript. J. Smothers and P. Ballhorn contributed to complete Figs. 1 and 2. S. Kottapalli, A.Ly and J. Villarreal contributed to data analysis and production of number of figures. We wish to thank Dr. Rong Li, Dr. Spudich, Dr. Bretscher, Dr. Tanaka, Dr. Gerst, Dr. Weisman and Sara Wong for yeast strains and plasmids.

Appendix A. Supplementary data

Supplementary material related to this article can be found, in the online version, at doi:https://doi.org/10.1016/j.ejcb.2020.151143.

References

Arlt, H., Reggiori, F., Ungermann, C., 2015. Retromer and the dynamin Vps1 cooperate in the retrieval of transmembrane proteins from vacuoles. J. Cell. Sci. 128, 645–655.
Bohl, F., Kruse, C., Frank, A., Ferring, D., Jansen, R.P., 2000. She2p, a novel RNA-binding protein tethers ASH1 mRNA to the Myo4p myosin motor via She3p. EMBO J. 19, 5514–5524.
Bretscher, A., 2003. Polarized growth and organelle segregation in yeast: the tracks, motors, and receptors. J. Cell Biol. 160, 811–816.
Brown, S.S., 1997. Myosins in yeast. Curr. Opin. Cell Biol. 9, 44–48.
Burda, P., Padilla, S.M., Sarkar, S., Emr, S.D., 2002. Retromer function in endosome-to-Golgi retrograde transport is regulated by the yeast Vps34 PtdIns 3-kinase. J. Cell. Sci. 115, 3889–3900.
Buss, F., Kendrick-Jones, J., 2011. Multifunctional myosin VI has a multitude of cargoes. Proc. Natl. Acad. Sci. U.S.A. 108, 5927–5928.
Catlett, N.L., Weisman, L.S., 1998. The terminal tail region of a yeast myosin-V mediates its attachment to vacuole membranes and sites of polarized growth. Proc. Natl. Acad. Sci. U.S.A. 95, 14799–14804.
Catlett, N.L., Duex, J.E., Tang, F., Weisman, L.S., 2000. Two distinct regions in a yeast myosin-V tail domain are required for the movement of different cargoes. J. Cell Biol. 150, 513–526.
Chen, D.C., Yang, B.C., Kuo, T.T., 1992. One-step transformation of yeast in stationary phase. Curr. Genet. 21, 83–84.
Chi, R.J., Liu, J., West, M., Wang, J., Odorizzi, G., Burd, C.G., 2014. Fission of SNX-BAR-coated endosomal retrograde transport carriers is promoted by the dynamin-related protein Vps1. J. Cell Biol. 204, 793–806.
Conibear, E., Stevens, T.H., 1998. Multiple sorting pathways between the late Golgi and the vacuole in yeast. Biochim. Biophys. Acta 1404, 211–230.
Cooper, A.A., Stevens, T.H., 1996. Vps10p cycles between the late-Golgi and prevacuolar compartments in its function as the sorting receptor for multiple yeast vacuolar hydrolases. J. Cell Biol. 133, 529–541.
Donovan, K.W., Bretscher, A., 2012a. Myosin-V is activated by binding secretory cargo and released in coordination with Rab/exocyst function. Dev. Cell 23, 769–781.
Donovan, Kirk W., Bretscher, A., 2012b. Myosin-V is activated by binding secretory cargo and released in coordination with Rab/Exocyst function. Dev. Cell 23, 769–781.
Eves, P.T., Jin, Y., Brunner, M., Weisman, L.S., 2012. Overlap of cargo binding sites on myosin V coordinates the inheritance of diverse cargoes. J. Cell Biol. 198, 69–85.
Fagarasanu, A., Mast, F.D., Knoblach, B., Jin, Y., Brunner, M.J., Logan, M.R., Glover, J.N. M., Eitzen, G.A., Aitchison, J.D., Weisman, L.S., et al., 2009. Myosin-driven peroxisome partitioning in S. cerevisiae. J. Cell Biol. 186, 541–554.
Furuta, N., Fujimura-Kamada, K., Saito, K., Yamamoto, T., Tanaka, K., 2007. Endocytic recycling in yeast is regulated by putative phospholipid translocases and the Ypt31p/32p-Rcy1p pathway. Mol. Biol. Cell 18, 295–312.
Galletta, B.J., Chuang, D.Y., Cooper, J.A., 2008. Distinct roles for Arp2/3 regulators in actin assembly and endocytosis. PLoS Biol. 6, e1.
Gerst, J.E., Rodgers, L., Riggs, M., Wigler, M., 1992. SNC1, a yeast homolog of the synaptic vesicle-associated membrane protein/synaptobrevin gene family: genetic interactions with the RAS and CAP genes. Proc. Natl. Acad. Sci. U.S.A. 89, 4338–4342.
Goodson, H.V., Anderson, B.L., Warrick, H.M., Pon, L.A., Spudich, J.A., 1996. Synthetic lethality screen identifies a novel yeast myosin I gene (MYO5): myosin I proteins are required for polarization of the actin cytoskeleton. J. Cell Biol. 133, 1277–1291.
Hettema, E.H., Lewis, M.J., Black, M.W., Pelham, H.R., 2003. Retromer and the sorting nexins Snx4/41/42 mediate distinct retrieval pathways from yeast endosomes. EMBO J. 22, 548–557.
Ishikawa, K., Catlett, N.L., Novak, J.L., Tang, F., Nau, J.J., Weisman, L.S., 2003. Identification of an organelle-specific myosin V receptor. J. Cell Biol. 160, 887–897.
Jansen, R.P., Dowzer, C., Michaelis, C., Galova, M., Nasmyth, K., 1996. Mother cell-specific HO expression in budding yeast depends on the unconventional myosin myo4p and other cytoplasmic proteins. Cell 84, 687–697.
Jin, Y., Sultana, A., Gandhi, P., Franklin, E., Hamamoto, S., Khan, A.R., Munson, M., Schekman, R., Weisman, L.S., 2011. Myosin V transports secretory vesicles via a Rab GTPase cascade and interaction with the exocyst complex. Dev. Cell 21, 1156–1170.
Kaksonen, M., Toret, C.P., Drubin, D.G., 2005. A modular design for the clathrin- and actin-mediated endocytosis machinery. Cell 123, 305–320.
Kama, R., Robinson, M., Gerst, J.E., 2007. Btn2, a Hook1 ortholog and potential Batten disease-related protein, mediates late endosome-Golgi protein sorting in yeast. Mol. Cell. Biol. 27, 605–621.
Kodera, N., Ando, T., 2014. The path to visualization of walking myosin V by high-speed atomic force microscopy. Biophys. Rev. 6, 237–260.
Lewellyn, E.B., Pedersen, R.T., Hong, J., Lu, R., Morrison, H.M., Drubin, D.G., 2015. An engineered minimal WASP-Myosin fusion protein reveals essential functions for endocytosis. Dev. Cell 35, 281–294.
Lillie, S.H., Brown, S.S., 1994. Immunofluorescence localization of the unconventional myosin, Myo2p, and the putative kinesin-related protein, Smy1p, to the same regions of polarized growth in Saccharomyces cerevisiae. J. Cell Biol. 125, 825–842.
Lipatova, Z., Tokarev, A.A., Jin, Y., Mulholland, J., Weisman, L.S., Segev, N., 2008. Direct interaction between a myosin V motor and the Rab GTPases Ypt31/32 is required for polarized secretion. Mol. Biol. Cell 19, 4177–4187.
Lister, I.M., Tolliday, N.J., Li, R., 2006. Characterization of the minimum domain required for targeting budding yeast myosin II to the site of cell division. BMC Biol. 4, 19.
Long, R.M., Gu, W., Lorimer, E., Singer, R.H., Chartrand, P., 2000. She2p is a novel RNA-binding protein that recruits the Myo4p-She3p complex to ASH1 mRNA. EMBO J. 19, 6592–6601.
Lord, M., Laves, E., Pollard, T.D., 2005. Cytokinesis depends on the motor domains of Myosin-II in fission yeast but not in budding yeast. Mol. Biol. Cell 16, 5346–5355.
Ma, M., Burd, C.G., Chi, R.J., 2017. Distinct complexes of yeast Snx4 family SNX-BARs mediate retrograde trafficking of Snc1 and Atg27. Traffic (Copenhagen, Denmark) 18, 134–144.
Marcusson, E.G., Horazdovsky, B.F., Cereghino, J.L., Gharakhanian, E., Emr, S.D., 1994. The sorting receptor for yeast vacuolar carboxypeptidase Y is encoded by the VPS10 gene. Cell 77, 579–586.
McIntosh, B.B., Ostap, E.M., 2016. Myosin-I molecular motors at a glance. J. Cell. Sci. 129, 2689–2695.
Musch, A., Cohen, D., Rodriguez-Boulan, E., 1997. Myosin II is involved in the production of constitutive transport vesicles from the TGN. J. Cell Biol. 138, 291–306.
Nickerson, D.P., West, M., Henry, R., Odorizzi, G., 2010. Regulators of Vps4 ATPase activity at endosomes differentially influence the size and rate of formation of intralumenal vesicles. Mol. Biol. Cell 21, 1023–1032.
Pashkova, N., Catlett, N.L., Novak, J.L., Weisman, L.S., 2005a. A point mutation in the cargo-binding domain of myosin V affects its interaction with multiple cargoes. Eukaryot. Cell 4, 787–798.
Pashkova, N., Catlett, N.L., Novak, J.L., Wu, G., Lu, R., Cohen, R.E., Weisman, L.S., 2005b. Myosin V attachment to cargo requires the tight association of two functional subdomains. J. Cell Biol. 168, 359–364.
Pashkova, N., Jin, Y., Ramaswamy, S., Weisman, L.S., 2006. Structural basis for myosin V discrimination between distinct cargoes. EMBO J. 25, 693–700.
Pierobon, P., Achouri, S., Courty, S., Dunn, A.R., Spudich, J.A., Dahan, M., Cappello, G., 2009. Velocity, processivity, and individual steps of single myosin V molecules in live cells. Biophys. J. 96, 4268–4275.
Piper, R.C., Cooper, A.A., Yang, H., Stevens, T.H., 1995. VPS27 controls vacuolar and endocytic traffic through a prevacuolar compartment in Saccharomyces cerevisiae. J. Cell Biol. 131, 603–617.
Pollard, L.W., Lord, M., 2014. Getting myosin-V on the right track: tropomyosin sorts transport in yeast. Bioarchitecture 4, 35–38.
Richman, T.J., Sawyer, M.M., Johnson, D.I., 2002. Saccharomyces cerevisiae Cdc42p localizes to cellular membranes and clusters at sites of polarized growth. Eukaryot. Cell 1, 458–468.
Ryan, J.M., Nebenfuhr, A., 2018. Update on myosin motors: molecular mechanisms and physiological functions. Plant Physiol. 176, 119–127.
Santiago, E., Akamine, P., Snider, J., Wong, V., Jessulat, M., Deineko, V., Gagarinova, A., Aoki, H., Minic, Z., Phanse, S., et al., 2016. Novel interactome of Saccharomyces cerevisiae myosin type II identified by a modified integrated membrane yeast two-hybrid (iMYTH) screen. G3 (Bethesda) 6, 1469–1474.
Santiago-Tirado, F.H., Legesse-Miller, A., Schott, D., Bretscher, A., 2011. PI4P and Rab inputs collaborate in myosin-V-dependent transport of secretory compartments in yeast. Dev. Cell 20, 47–59.
Schmidt, M., Bowers, B., Varma, A., Roh, D.H., Cabib, E., 2002. In budding yeast, contraction of the actomyosin ring and formation of the primary septum at cytokinesis depend on each other. J. Cell. Sci. 115, 293–302.
Schott, D., Ho, J., Pruyne, D., Bretscher, A., 1999. The COOH-terminal domain of Myo2p, a yeast myosin V, has a direct role in secretory vesicle targeting. J. Cell Biol. 147, 791–808.

Schott, D.H., Collins, R.N., Bretscher, A., 2002. Secretory vesicle transport velocity in living cells depends on the myosin-V lever arm length. J. Cell Biol. 156, 35–39.
Sun, Y., Martin, A.C., Drubin, D.G., 2006. Endocytic internalization in budding yeast requires coordinated actin nucleation and myosin motor activity. Dev. Cell 11, 33–46.
Suzuki, S.W., Emr, S.D., 2018. Membrane protein recycling from the vacuole/lysosome membrane. J. Cell Biol. 217, 1623–1632.
Takeda, M., Yamagami, K., Tanaka, K., 2014. Role of phosphatidylserine in phospholipid flippase-mediated vesicle transport in Saccharomyces cerevisiae. Eukaryot. Cell 13, 363–375.
TerBush, D.R., Maurice, T., Roth, D., Novick, P., 1996. The Exocyst is a multiprotein complex required for exocytosis in Saccharomyces cerevisiae. EMBO J. 15, 6483–6494. Dec 02.
Tolliday, N., Pitcher, M., Li, R., 2003. Direct evidence for a critical role of myosin II in budding yeast cytokinesis and the evolvability of new cytokinetic mechanisms in the absence of myosin II. Mol. Biol. Cell 14, 798–809.
Trybus, K.M., 2008. Myosin V from head to tail. Cell. Mol. Life Sci. 65, 1378–1389.
Vagnozzi, A.N., Pratico, D., 2019. Endosomal sorting and trafficking, the retromer complex and neurodegeneration. Mol. Psychiatry 24, 857–868.
Valdez-Taubas, J., Pelham, H.R., 2003. Slow diffusion of proteins in the yeast plasma membrane allows polarity to be maintained by endocytic cycling. Curr. Biol. 13, 1636–1640.
Valiathan, R.R., Weisman, L.S., 2008. Pushing for answers: is myosin V directly involved in moving mitochondria? J. Cell Biol. 181, 15–18.
Walch-Solimena, C., Collins, R.N., Novick, P.J., 1997. Sec2p mediates nucleotide exchange on Sec4p and is involved in polarized delivery of post-Golgi vesicles. J. Cell Biol. 137, 1495–1509.
Warner, C.L., Stewart, A., Luzio, J.P., Steel, K.P., Libby, R.T., Kendrick-Jones, J., Buss, F., 2003. Loss of myosin VI reduces secretion and the size of the Golgi in fibroblasts from Snell's Waltzer mice. EMBO J. 22, 569–579.
Weisman, L.S., 2006. Organelles on the move: insights from yeast vacuole inheritance. Nat. Rev. Mol. Cell Biol. 7, 243–252.
Winding, M., Gelfand, V.I., 2014. Breaking up isn't easy: myosin V and its cargoes need Dma1 ubiquitin ligase's help. Dev. Cell 28, 479–480.
Woodman, S., Kim, K., 2018. Membrane Lipids: implication for diseases and membrane trafficking. SM J. Biol. 3, 1–5.
Yanguas, F., Moscoso-Romero, E., Valdivieso, M.H., 2019. Ent3 and GGA adaptors facilitate diverse anterograde and retrograde trafficking events to and from the prevacuolar endosome. Sci. Rep. 9, 10747.
Yau, R.G., Peng, Y., Valiathan, R.R., Birkeland, S.R., Wilson, T.E., Weisman, L.S., 2014. Release from myosin V via regulated recruitment of an E3 ubiquitin ligase controls organelle localization. Dev. Cell 28, 520–533.